Letter

One-kiloparsec expanding cylinder of H I gas around the Galactic Center

Yoshiaki SOFUE*

Institute of Astronomy, The University of Tokyo, 2-21-1 Osawa Mitaka, Tokyo 181-0015, Japan

*E-mail: sofue@ioa.s.u-tokyo.ac.jp

Abstract

We report the discovery of an expanding cylinder of H I gas of radius 1 kpc and vertical extent 800 pc by analyzing the 21 cm line survey data from the literature. The cylinder is expanding at 150 km s^{-1}, rotating at 100 km s^{-1}, and is interpreted as due to a high-velocity conical wind from the Galactic Center. The total mass of the cylinder is estimated to be $\sim$8.5 $\times$ 10^5 $M_{\odot}$ and kinetic energy $\sim$3 $\times$ 10^{53} erg.

Key words: ISM: atoms — ISM: jets and outflows — Galaxy: center — Galaxy: kinematics and dynamics

1 Introduction

Expanding rotating rings and cylinders concentric to the Galactic Center (GC) have been observed at various radii in the Galactic disc in the radio line emissions, exhibiting tilted ellipses in longitude–radial velocity diagrams (LVD). The 3 kpc and 2.4 kpc expanding rings were discovered as tilted LV ellipses by the early H I line observations (Sanders & Wrixon 1972, 1973; Simonson & Mader 1973). A cavity in the halo having conical boundary has been found in the H I halo indicating a galactic wind from the GC (Lockman & McClure-Griffiths 2016; Lockman et al. 2020; Sofue 2017b, 2022). The 200 pc expanding molecular ring (EMR) has been known as the evidence for the GC explosive activity (Kaifu et al. 1972; Scoville 1972; Sofue 1995a, 1995b, 2017a; Krumholz et al. 2017). In these observational studies, the tilted LV ellipse has been interpreted as due to expansion of a ring or cylinder rotating around the GC.

On the other hand, dynamical studies of the Galactic disc with a bar potential have shown that the bar-induced non-circular motion of gas along the X orbits can also explain the tilted ellipses and parallelograms in the LVD (Binney

et al. 1991; Sormani & Magorrian 2015; Rodriguez-Fernandez & Combes 2008). It is, therefore, controversial whether the LV ellipses are due to expanding motion or non-circular flow in a bar potential.

In this paper, we present a new case of LV ellipse at high latitudes, which cannot be explained by a bar potential model, but is naturally attributed to an expanding gas flow from the GC.

2 Tilted ellipse in longitude–velocity diagram

In figure 1a we show H I-line LVD in the central $40° \times 10°$ region, each averaged within latitudinal interval of $1°$ in the central $l = \pm 20°$ region, as produced from the H I Galactic All Sky Survey (GASS) (McClure-Griffiths et al. 2009; HI4PI Collaboration 2016). Besides the bright disc structures near the galactic plane and the concentrated GC disc, we notice the vertically extended, tilted, and curved ridges at latitudes $|b| \geq \sim 2°$ at $l \sim \pm 5°$–$10°$. Although fainter than the disc structures, they are clearly visible with brightness of $T_b \sim 1$–5 K, showing large non-circular motions. The features are also visible in the higher-resolution H I

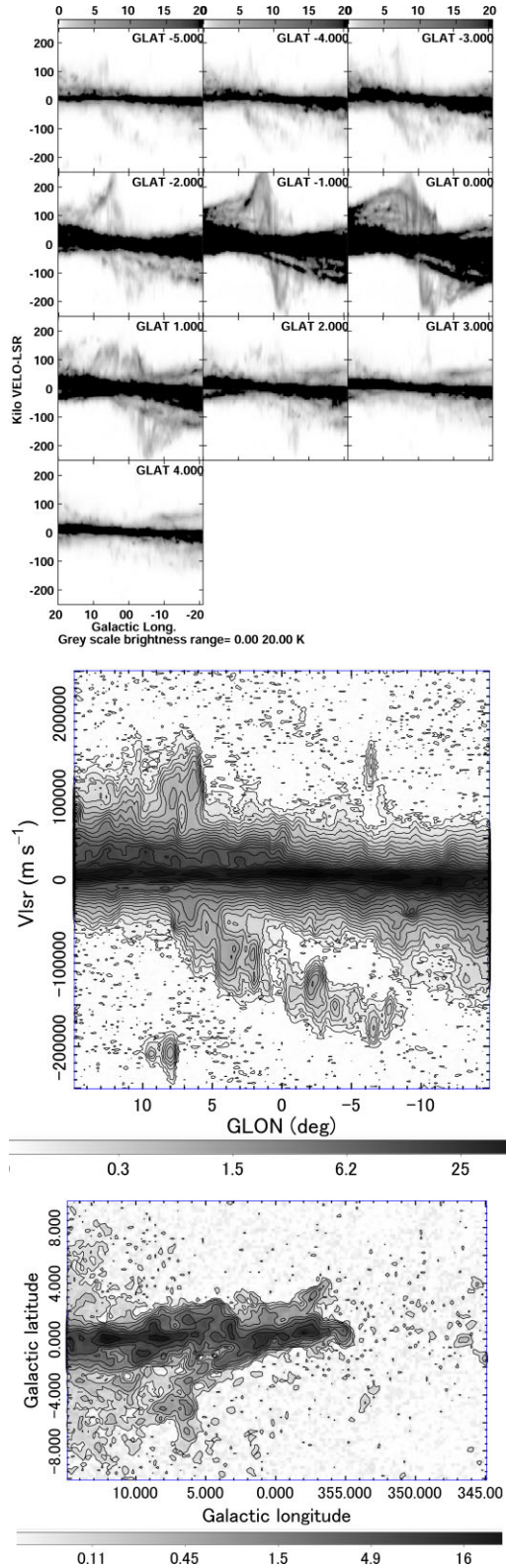**Fig. 2.** H I LVD averaged in $2° \leq |b| \leq 4°$ ($|h| = 280$–560 pc).

Fig. 1. (a) H I-line LVD of the central $40° \times 10°$ region, each averaged within every $1°$ latitudinal interval between $b = -5°$ and $-4°$ (top left) to $+4°$ and $+5°$ (bottom right). (b) Enlargement of LVD averaged between $b = -5°$ to $-4°$. (c) T_b channel map at $V_{LSR} = +120$ km s^{-1}.

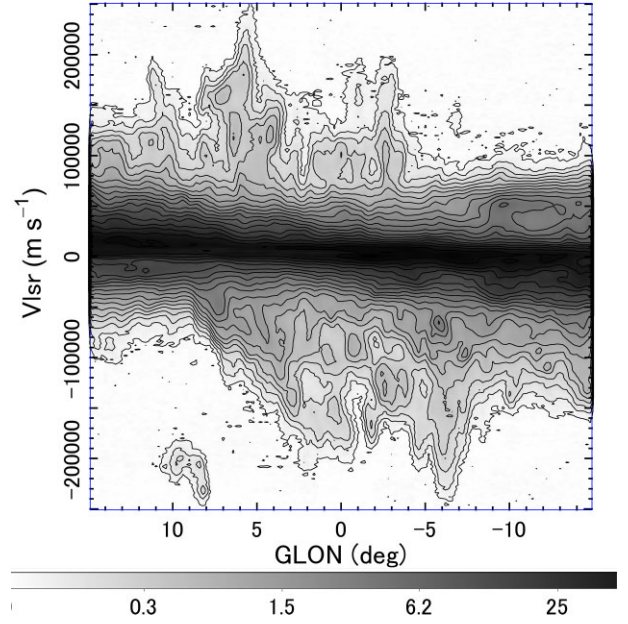survey of the central $\pm 10°$ region (McClure-Griffiths et al. 2012). In the intensity channel maps, the H I disc near the tangent velocities at $V_{LSR} \sim \pm -100$–200 km s^{-1} exhibits vertically extended spurs, some of which correspond to the non-circular LV ridges.

Figure 1b enlarges the LVD at $b = -4°.5$ ($h \sim -630$ pc), where a curved ridge composing a part of an LV ellipse clearly shows up, revealing high non-circular velocities. Figure 1c shows a T_b channel map at $V_{LSR} = +120$ km s^{-1}, representing the gas distribution on the sky at this velocity. It reveals a obliquely extending spur toward the south-east corresponding to the left-hand-side edge of the LV ellipse in the top panel.

Figure 2 shows an LV diagram averaged at $2° \leq |b| \leq 4°$, or at vertical heights from $|h| = 280$ to 560 pc. The vertically extended, tilted and curved LV ridge shows up clearly here, composing a coherent tilted ellipse centered on the GC. The maximum and minimum velocities along the ellipse are $V_{LSR} \sim \pm 250$ km s^{-1} and the longitudinal extent is $l \sim \pm 7°.5$ (± 1.0 kpc). The intersections of the ellipse with the rotation axis of the Galaxy at $l = 0°$ occur at $V_{LSR} \sim \pm 150$ km s^{-1}, indicating that the ellipse is expanding at this velocity. The tangential velocity at the maximum longitudes appears at $V_{LSR} \sim \pm 100$ km s^{-1}, indicating that the ring is rotating at ~ 100 km s^{-1} in the same direction as that of the galactic rotation. The H I intensity attains the maximum at the left- and right-hand-side edges of the ellipse, and a minimum or lacking region appears near the rotation axis. Another noticeable point is the isolation of the LV ellipse, uniquely standing alone surrounded by emission vacancy along the terminal-velocity envelope.

Using the diagram, we then estimate the mass of the ellipse, assuming that the distance to the GC is 8 kpc. First we measure the mean brightness temperature T_b at velocities higher than $|V_{LSR}| \leq 75$ km s^{-1} in order to avoid the Galactic disc's emission. By multiplying the velocity channel width and grid interval to the obtained total counts of T_b, we calculate the mass of the measured area to be $M_{measured} \sim 2.4 \times 10^5 M_\odot$. Here, we used a conversion factor of $X_{HI} = 1.823 \times 10^{18}$ H cm^{-2} [K km s^{-1}]$^{-1}$ and the mean atomic weight including metals per hydrogen of $\mu = 1.4$. The thus-estimated mass represents a value appearing in figure 2, partially filling the whole structure by a factor of $\eta \sim 4°/10° \times (400 - 150)$ km s^{-1}/400 km s^{-1} ~ 0.32. Thus, we correct for the filling factor, and obtain the total gaseous mass composing the LV ellipse to be $M_{tot} \sim M_{measured}/\eta \sim 8.5 \times 10^5 M_\odot$.

3 Discussion and summary

The H I ellipse in the LV diagram can be traced up to latitudes as high as $b \sim \pm 5°$, or $h \sim \pm 800$ pc from the galactic plane. From the brightness temperature of $T_b \sim 2$ K and velocity width $\delta v \sim 30$ km s^{-1}, the H I column density at this height is estimated to be $N_{HI} \sim 10^{20}$ H cm^{-2}. This yields a volume density of $n_{HI} \sim 0.1$ H cm^{-3} for a supposed line-of-sight depth of ~ 300 pc. The density is three orders of magnitudes higher than that of the H I Galactic disc of 10^{-4} H cm^{-3} and two orders of magnitudes higher than the warm H I disc of 10^{-3} H cm^{-3} at the same height (Sofue 2019). Even if the gas is galactic-shock compressed by a factor of 10, the density is higher than that of the disc or an arm by an order of magnitude or more. This means that the LV ellipse is not an extension of arm and/or ring structures associated with the Galactic disc. Furthermore, the stellar bulge and bar density at this height is an order of magnitude lower than that in the disc (Dwek et al. 1995), which means that the bar potential there is too shallow to produce the observed non-circular velocities of ~ 100km s^{-1}.

From these considerations, we may conclude that dynamical models incorporating bar-induced oval orbits of the disc gas may be excluded as an explanation of the observed non-circular motion in the high-latitude LV ellipse. This conclusion is confirmed by a detailed comparison of figures 1 and 2 with the simulated LV patterns around $l \sim \pm 8°$ in the most extensive LVD study of bar-induced non-circular flows in the galactic plane by two-dimensional treatment (Sormani & Magorrian 2015).

An alternate model to explain the non-circular LVD is an expanding ring or cylinder model of gaseous outflow driven by explosion and/or high-speed wind from the GC. In the following, we stand on this model, and estimate the parameters of the expanding motion. As estimated by fitting to the
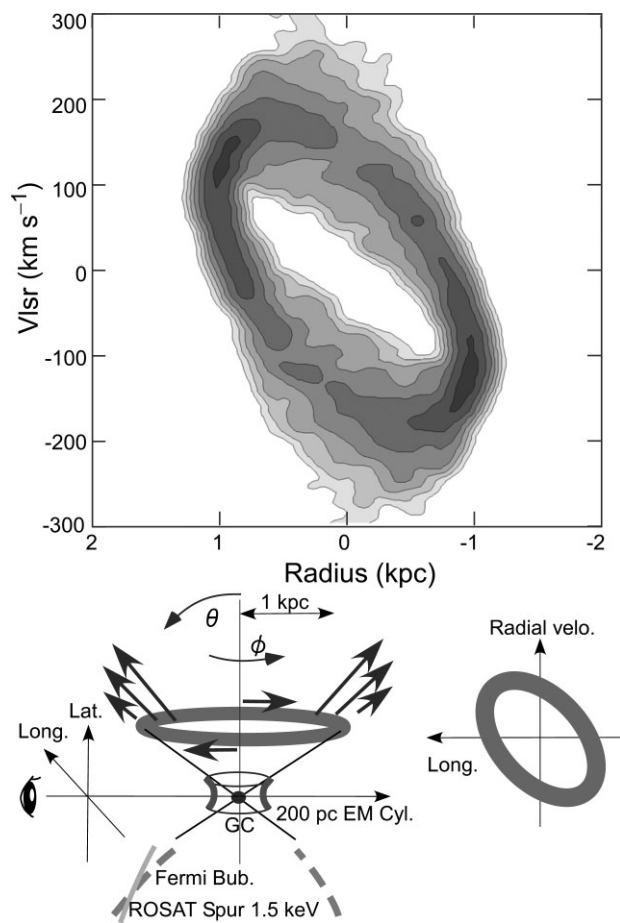

Fig. 3. Simulated LVD of the conical cylinder wind of H I gas and illustration of the parameters. Note the difference from LVD of an expanding ring showing uniform brightness as illustrated in the bottom right.

LV ellipse, the ring radius, expansion velocity, and rotation velocity are ~ 1 kpc, ~ 150 km s^{-1}, and 100 km s^{-1}, respectively. In the expanding ring model, the rotation slower than the galactic rotation of ~ 200 km s^{-1} is attributed to the conservation of angular momentum, because the gas is accumulated from the inner region by wind or a shock wave from the GC.

The observed LVD in figure 2 shows significant intensity variation along the ellipse in such a sense that the intensity attains maximum in the left- and right-hand-side edges, and minimum, or even is missing, around $l \sim 0°$. We recall that such a non-uniform LV ellipse can be explained by an outflow with variable expanding velocity (Sofue 2022). We here examine a simple case of a varying flow velocity model, where the line-of-sight velocity is given by

$$V = V_0(1 + \delta)e^{1-(r/r_0)^2}\sin\theta\sin\phi + V_{rot}\cos\phi, \quad (1)$$

where δ is fractional velocity dispersion with respect to V_0, r is the radius, θ is the opening angle of the wind from the z-axis, and ϕ is the azimuth angle of the element around

the rotation axis. Here, V_0 and r_0 are constants taken to be 100 km s^{-1} and 1 kpc, respectively, and *delta* is taken to be 0.5. The radial distribution of gas density is expressed by

$$\rho = \rho_0 e^{-[(r-r_0)/\Delta r]^2}, \tag{2}$$

where ρ_0 is the density at $r_0 = 1 \text{ kpc}$ and $\Delta r = 0.2 r_0$ is its width. From the height-to-radius ratio of the LV ellipse of $5°$ to $7°.5$, we calculate the opening angle of the cone from the rotation axis to be $\theta \sim 56°$. Then the measured velocity of $V_{\text{LSR}} = \pm 150 \text{ km s}^{-1}$ at $l \sim 0°$ yields a flow velocity of $V_0 \sim 180 \text{ km s}^{-1}$.

Figure 3 shows the calculated result with an illustration of the model. The simulation well reproduces the observed characteristics of LV ellipse as follows:

- Tilted LV ellipse fitted by $V_{\text{flow}} \sim 180 \text{ km s}^{-1}$ and $V_{\text{rot}} \sim 100 \text{ km s}^{-1}$.
- Intensity maximum on the left- and right-hand-side edges of the ellipse.
- Intensity minimum near $l = 0°$.

However, the lopsidedness as observed in figure 2 is not reproduced by the present model, which may be attributed to localized density distributions and/or to the asymmetric wind from the GC.

From the adopted parameters, we can estimate the total kinetic energy of the expanding motion of the ellipse to be $E_{\text{expa}} \sim 3 \times 10^{53}$ erg. The time scale for the expanding gas to reach the radius of ~ 1 kpc from the GC is of the order of $t \sim r/V_{\text{flow}} \sim 1 \text{kpc}/180 \text{ km s}^{-1} \sim 6$ Myr. These may be compared with the energy of $\sim 10^{55}$ erg of the strongest GC activity associated with several to 10 kpc scale giant bubbles in radio, X-, and γ-rays with a time scale of ~ 10 Myr (Kataoka et al. 2018). The H I wind may be one of intermittent minor events among the outflows from the GC.

On the sky, the root of the H I cone roughly coincides with the ridges of the Fermi bubbles and an X-ray "claw" (Su et al. 2010; Kataoka et al. 2015), and appears to be a continuation of the more central expanding molecular cone of 200 pc radius (Sofue 2017b), as illustrated in figure 3. The present outflow model is consistent with the current wind models (McClure-Griffiths et al. 2013; Lockman et al. 2016, 2020; Bland-Hawthorn & Cohen 2023; Sofue 2017b; Sofue & Kataoka 2021), providing complimentary physical quantities such as the flow and rotation velocities and the energy.

Data availability

The H I-line data were downloaded from ⟨https://www.atnf.csiro.au/research/GASS/index.html⟩.

Conflict of interest

There is no conflict of interest.

References

Binney, J., Gerhard, O. E., Stark, A. A., Bally, J., & Uchida, K. I. 1991, MNRAS, 252, 210

Bland-Hawthorn, J., & Cohen, M. 2003, ApJ, 582, 246

Dwek, E., et al. 1995, ApJ, 445, 716

HI4PI Collaboration 2016, A&A, 594, A116

Kaifu, N., Kato, T., & Iguchi, T. 1972, Nature Phys. Sci., 238, 105

Kataoka, J., Sofue, Y., Inoue, Y., Akita, M., Nakashima, S., & Totani, T. 2018, Galaxy, 6, 27

Kataoka, J., Tahara, M., Totani, T., Sofue, Y., Inoue, Y., Nakashima, S., & Cheung, C. C. 2015, ApJ, 807, 77

Krumholz, M. R., Kruijssen, J. M. D., & Crocker, R. M. 2017, MNRAS, 466, 1213

Lockman, F. J., & McClure-Griffiths, N. M. 2016, ApJ, 826, 215

Lockman, F. J., Di Teodoro, E. M., & McClure-Griffiths, N. M. 2020, ApJ, 888, 51

McClure-Griffiths, N. M., et al. 2009, ApJS, 181, 398

McClure-Griffiths, N. M., Dickey, J. M., Gaensler, B. M., Green, A. J., Green, J. A., & Haverkorn, M. 2012, ApJS, 199, 12

McClure-Griffiths, N. M., Green, J. A., Hill, A. S., Lockman, F. J., Dickey, J. M., Gaensler, B. M., & Green, A. J. 2013, ApJ, 770, L4

Rodriguez-Fernandez, N. J., & Combes, F. 2008, A&A, 489, 115

Sanders, R. H., & Wrixon, G. T. 1972, A&A, 18, 92

Sanders, R. H., & Wrixon, G. T. 1973, A&A, 26, 365

Scoville, N. Z. 1972, ApJ, 175, L127

Simonson, S. C., & Mader, G. L. 1973, A&A, 27, 337

Sofue, Y. 1995a, PASJ, 47, 527

Sofue, Y. 1995b, PASJ, 47, 551

Sofue, Y. 2017a, MNRAS, 470, 1982

Sofue, Y. 2017b, PASJ, 69, L8

Sofue, Y. 2019, MNRAS, 484, 2954

Sofue, Y. 2022, MNRAS, 509, 5809

Sofue, Y., & Kataoka, J. 2021, MNRAS, 506, 2170

Sormani, M. C., & Magorrian, J. 2015, MNRAS, 446, 4186

Su, M., Slatyer, T. R., & Finkbeiner, D. P. 2010, ApJ, 724, 1044